

Thick disc molecular gas fraction in NGC 6946

Narendra Nath Patra¹ \star

¹ Raman Research Institute, C. V. Raman Avenue, Sadashivanagar, Bengaluru 560080, India

ABSTRACT

Several recent studies reinforce the existence of a thick molecular disc in galaxies along with the dynamically cold thin disc. Assuming a two-component molecular disc, we model the disc of NGC 6946 as a four-component system consisting of stars, HI, thin disc molecular gas, and thick disc molecular gas in vertical hydrostatic equilibrium. Following, we set up the joint Poisson-Boltzmann equation of hydrostatic equilibrium and solve it numerically to obtain a three-dimensional density distribution of different baryonic components. Using the density solutions and the observed rotation curve, we further build a three-dimensional dynamical model of the molecular disc and consecutively produce simulated CO spectral cubes and spectral width profiles. We find that the simulated spectral width profiles distinguishably differ for different assumed thick disc molecular gas fractions. Several CO spectral width profiles are then produced for different assumed thick disc molecular gas fractions and compared with the observed one to obtain the best fit thick disc molecular gas fraction profile. We find that the thick disc molecular gas fraction in NGC 6946 largely remains constant across its molecular disc with a mean value of 0.70 ± 0.09 . We also estimate the amount of extra-planar molecular gas in NGC 6946. We find $\sim 50\%$ of the total molecular gas is extra-planar at the central region, whereas this fraction reduces to $\sim 15\%$ at the edge of the molecular disc. With our method, for the first time, we estimate the thick disc molecular gas fraction as a function of radius in an external galaxy with sub-kpc resolution.

Key words: ISM: molecules – molecular data – galaxies: structure – galaxies: kinematics and dynamics – galaxies: spiral

1 INTRODUCTION

The molecular gas in galaxies acts as the raw fuel for star formation, and hence, it can significantly influence the physical and chemical evolution of the interstellar medium (ISM). The neutral hydrogen (HI), on the other hand, plays the role of a long-term reservoir for star formation. The stars form out of molecular clouds, which itself is produced from the Cold Neutral Medium (CNM) phase of the atomic ISM. In that sense, the HI and the molecular gas closely related to star formation in spiral galaxies such as the star formation and the total gas surface densities (HI+molecular) in these galaxies are found to be tightly correlated to each other (Schmidt 1959; Kennicutt 1998; Bigiel et al. 2008; Leroy et al. 2009a). However, in smaller dwarf galaxies, this relation could be complicated as there is no significant detection of molecular gas despite great efforts (see, e.g., Taylor, Kobulnicky & Skillman 1998; Schruba et al. 2012). Even though the star formation in these galaxies is found to correlate with the HI and, the CNM surface densities (Bigiel et al. 2010; Roychowdhury et al. 2009, 2011, 2014; Roychowdhury, Chengalur & Shi 2017; Patra et al. 2016). Hence, it is essential to investigate the ISM conditions of the HI/molecular gas, which can directly influence the star formation. For example, in a recent

study, Bacchini et al. (2019) has revealed that the traditional Kennicutt-Schmidt law (KS law, relation between gas surface density and the star formation rate surface density (SFR), Kennicutt (1998)) shows much less scatter when the SFR is compared with the volume density of the gas (HI+molecular) instead of surface densities. This indicates that the volume density of the gas is more closely related to SFR than the surface densities, and hence, the determination of a three-dimensional distribution of the same would be imperative to understand the connection between gas and star formation.

The molecular disc in galaxies is thought to be a dynamically cold component settled very close to the midplane, having a very low kinetic temperature (a few tens of Kelvin). This demands the scale height, and the physical extent of the molecular gas in galaxies would be restricted to much lower heights as compared to the HI disc. However, many direct observations of the edge-on galaxy NGC 891 reveal a substantial amount of extraplanar gas and dust reaching up to heights of several kiloparsecs from the midplane. For example, in a deep Westerbork Synthesis Radio Telescope (WSRT) observation, Fraternali et al. (2005) detected a significant amount of extraplanar HI with a scale height of ~ 3 kpc (see also Swaters, Sancisi & van der Hulst 1997; Fraternali & Binney 2006). Similarly, several others performed deep $H\alpha$ observations and traced the extraplanar diffused ionized gas in NGC 891 to a height as large as $\sim 4 - 5$

\star E-mail: narendra@rri.res.in

kpc (typical scale height of ~ 1 kpc) (Dettmar 1990; Rand & Kulkarni 1990; Hoopes, Walterbos & Rand 1999; Kamphuis et al. 2007b; Boettcher et al. 2016). Further, deep UV (scattered by dust) observations confirmed the presence of dust at heights ~ 2 kpc from the midplane (Howk & Savage 2000; Rossa et al. 2004; Kamphuis et al. 2007a; Seon et al. 2014).

Garcia-Burillo et al. (1992) detected molecular gas in NGC 891 at $\sim 1 - 1.4$ kpc above the midplane. The scale height of the molecular gas in a thin disc is expected to be a few hundred parsecs. Not only that, recent high spatial and spectral studies also provide adequate evidence that the molecular gas in galaxies can also exist in a thick disc with much larger scale heights. For example, Caldú-Primo et al. (2013) used the data of 12 nearby large spiral galaxies from The HERA CO Line Extragalactic survey (HERACLES, Leroy et al. (2009b)) and The HI Nearby Galaxy Survey (THINGS, Walter et al. (2008)) to stack the HI and the CO spectra in these galaxies and found that the ratio, $\sigma_{HI}/\sigma_{CO} = 1.0 \pm 0.2$ with $\sigma_{HI} = 11.9 \pm 3.1$ km s $^{-1}$. Later, Mogotsi et al. (2016) used the same data to identify the high SNR regions in both the HI and CO map and compared the velocity dispersions. They found a $\sigma_{HI}/\sigma_{CO} = 1.4 \pm 0.2$ with $\sigma_{HI} = 11.7 \pm 2.3$ km s $^{-1}$. These studies conclude that the molecular gas in galaxies exists in two phases/discs. One in a thin disc close to the midplane and has a low velocity dispersion (thin disc molecular gas). The other one exists in a more diffuse thick disc with a velocity dispersion the same as σ_{HI} (thick disc molecular gas). Due to the diffuse nature of the thick disc molecular gas, it is not detected in the individual spectra, whereas it shows its signature in a high SNR stacked spectrum.

The existence of this diffuse molecular disc in galaxies raises several vital questions. For example, what is the origin of this low density diffuse molecular gas? As they have the same velocity dispersion as the HI, the thick disc molecular gas will have a similar scale height as the HI disc. In that sense it is unclear how this phase can survive at these heights from the midplane, where the metagalactic radiation is high. However, several earlier studies revealed the existence of dust in galaxies at a considerable height from the midplane (Howk & Savage 2000; Rossa et al. 2004; Kamphuis et al. 2007a; Seon et al. 2014; Shinn 2018; Jo et al. 2018). This dust could, in principle, provide enough shielding to this diffuse molecular disc. Nevertheless, the origin and physical conditions for such molecular phase substance at a considerable height are not yet clearly understood.

Several studies point towards a dynamical origin of the diffuse molecular gas in spiral galaxies. For example, it is proposed that due to the passage of the spiral density wave, there could be a spontaneous conversion of the atomic phase into the diffuse molecular phase (Blitz & Shu 1980; Cohen et al. 1980; Scoville & Hersh 1979; Heyer & Dame 2015). On the other hand, some studies suggest that the diffuse molecular gas already exists in the form of small molecular clouds, which are not detected within individual beams. The observed Giant Molecular Clouds (GMCs) in the arm then can be produced by dynamically induced coagulation due to the passage of the density wave (Scoville & Hersh 1979; Vogel, Kulkarni & Scoville 1988; Hartmann, Ballesteros-Paredes & Bergin 2001; Kawamura et al. 2009; Koda et al. 2011; Miura et al. 2012; Pety et al. 2013; Koda, Scoville & Heyer 2016). However, these studies cannot provide a satisfactory explanation of the substantial amount of extraplanar molecular gas at considerable heights.

On the other hand, a number of high-resolution, sensitive observations revealed significant molecular outflows in galaxies due to enhanced star formation or Active Galactic Nuclei (AGN) activities. These molecular outflows can carry a signif-

icant amount of molecular gas and energy to produce the observed extraplanar molecular gas comfortably. For example, using CO observations, Weiß et al. (1999) detected a molecular superbubble in M82 having a diameter of ~ 130 pc, which has broken out into the Cicum Galactic Medium (CGM). Employing simple theoretical models, they infer that a supernovae rate of ~ 0.001 per year would be sufficient to produce this kind of superbubbles. Walter, Weiss & Scoville (2002) observed molecular streamers in M82 using high resolution (~ 70 pc) CO observations. These streamers are believed to be closely related to the starburst activity in the galaxy and can expel molecular gas to heights ~ 1.2 kpc. Feruglio et al. (2010) observed Mrk 231, a nearby quasar using the Plateau de Bure interferometer (PdBI), and found a substantial amount of molecular outflow from the central region. Likewise, several other studies also found evidence of starburst or AGN driven outflows leading the molecular gas to large heights (Sakamoto, Ho & Peck 2006; Alatalo et al. 2011; Salak et al. 2013; Bolatto et al. 2013; Krieger et al. 2019; Salak et al. 2020). These mechanisms could be viable pathways for producing and maintaining the observed diffuse (extraplanar) molecular gas in galaxies.

Though the detection of the diffuse molecular discs in galaxies has become less ambiguous with recent sensitive observations, its physical properties are largely unknown. For example, what is the fractional abundance of this component in galaxies? How does this fraction vary with radius? Pety et al. (2013) observed the nearby large spiral galaxy M51 with the Plateau de Bure Interferometer (PdBI) to map its molecular disc with an unprecedented spatial resolution of ~ 40 pc. They also used the data from the IRAM 30 m telescope to map the galaxy with a single-dish. They find that the single-dish observation recovers almost twice the flux detected by the PdBI interferometer. They concluded that the diffuse thick disc molecular gas is resolved out in the high spatial resolution interferometric observation, which is detected in low-resolution single-dish measurement. Comparing the fluxes detected in single-dish and the interferometric observations, they infer at least 50% of the molecular gas in M51 is in the thick disc. However, this kind of measurement is global; i.e., it does not provide any information on how this fraction varies within a galaxy as a function of different physical conditions. Not only that, this kind of estimation requires high spatial resolution interferometric observation along with a single-dish measurement, which very often is not available simultaneously.

In this paper, we develop a method to estimate the thick disc molecular gas fraction as a function of radius in external galaxies and apply it to a nearby large spiral galaxy NGC 6946. We model the baryonic disc of the galaxy as a four-component system consisting of stars, HI and two molecular discs (thin and thick). We assume that these discs are in vertical hydrostatic equilibrium under their mutual gravity in the external force field of the dark matter halo. Under these assumptions, we set up the joint Poisson-Boltzmann equation of hydrostatic equilibrium and solve it numerically. With these solutions, we build a three-dimensional dynamical model of the molecular disc in NGC 6946 and produce CO spectral cubes and spectral width profiles equivalent to the observation. We find that these obtained spectral widths are sensitive to the assumed thick disc molecular gas fraction at every radius. Utilizing this characteristic, we produce a number of spectral cubes and hence spectral width profiles with different thick disc molecular gas fractions and compare it with the observed profile to constrain the thick disc molecular gas fraction in NGC 6946 as a function of radius.

2 MODELING THE DISC OF NGC 6946

As mentioned above, we construct several model molecular discs for NGC 6946 with different thick disc molecular gas fraction, f_{tk} , and produce expected spectral width profiles for all of them. To do that, we model the baryonic disc in NGC 6946 as a four-component system consisting of stars, HI, thick disc molecular gas, and thin disc molecular gas. We assume that all these discs are in vertical hydrostatic equilibrium. For simplicity, we consider all the discs are coplanar and concentric. With these assumptions, the Poisson's equation of hydrostatic equilibrium in cylindrical polar coordinate can be written as

$$\frac{1}{R} \frac{\partial}{\partial R} \left(R \frac{\partial \Phi_{\text{total}}}{\partial R} \right) + \frac{\partial^2 \Phi_{\text{total}}}{\partial z^2} = 4\pi G \left(\sum_{i=1}^4 \rho_i + \rho_h \right) \quad (1)$$

where Φ_{total} is the total potential due to all the baryonic components and the dark matter halo. ρ_i represents the volume density of the disc components where i runs for stars (ρ_s), HI (ρ_{HI}), thin disc molecular gas ($\rho_{\text{H2},\text{tn}}$) and thick disc molecular gas ($\rho_{\text{H2},\text{tk}}$). ρ_h denotes the density of the dark matter halo. For this modeling, we consider the dark matter halo to provide a fixed potential (not live), which is determined by the mass-modeling of the observed rotation curve.

The total potential, Φ_{total} , is not a directly measurable quantity, and hence, Eq. 1 can not be solved in its present form. Instead, we use the Boltzmann equation, to replace the Φ_{total} with a more directly measurable quantity, vertical velocity dispersion. In hydrostatic equilibrium, the gradient in pressure will be balanced by the gradient in the total potential. Hence,

$$\frac{\partial}{\partial z} (\rho_i \langle \sigma_z^2 \rangle_i) + \rho_i \frac{\partial \Phi_{\text{total}}}{\partial z} = 0 \quad (2)$$

Where $\langle \sigma_z \rangle_i$ is the vertical velocity dispersion of the i^{th} disc component. Eq. 2 can be used to simplify Eq. 1 such as,

$$\begin{aligned} \langle \sigma_z^2 \rangle_i \frac{\partial}{\partial z} \left(\frac{1}{\rho_i} \frac{\partial \rho_i}{\partial z} \right) = & \\ & - 4\pi G (\rho_s + \rho_{\text{HI}} + \rho_{\text{H2},\text{tn}} + \rho_{\text{H2},\text{tk}} + \rho_h) \\ & + \frac{1}{R} \frac{\partial}{\partial R} \left(R \frac{\partial \Phi_{\text{total}}}{\partial R} \right) \end{aligned} \quad (3)$$

Assuming the HI rotation curve traces the total gravitational potential reasonably accurately, the last term in the above equation can be computed as

$$\left(R \frac{\partial \Phi_{\text{total}}}{\partial R} \right)_{R,z} = (v_{\text{rot}}^2)_{R,z} \quad (4)$$

Putting Eq. 4 in Eq. 3, we get the final hydrostatic equilibrium equation as

$$\begin{aligned} \langle \sigma_z^2 \rangle_i \frac{\partial}{\partial z} \left(\frac{1}{\rho_i} \frac{\partial \rho_i}{\partial z} \right) = & \\ & - 4\pi G (\rho_s + \rho_{\text{HI}} + \rho_{\text{H2},\text{tn}} + \rho_{\text{H2},\text{tk}} + \rho_h) \\ & + \frac{1}{R} \frac{\partial}{\partial R} (v_{\text{rot}}^2) \end{aligned} \quad (5)$$

Eq. 5 represents four coupled second-order partial differential equations in ρ_s , ρ_{HI} , $\rho_{\text{H2},\text{tn}}$, and $\rho_{\text{H2},\text{tk}}$. The solutions of this equation at a radius will provide the density distribution of the different disc components as a function of the vertical height

(z) from the midplane. To obtain a complete three-dimensional density distribution of the disc components, one needs to solve Eq. 5 at all radii. However, several input parameters are needed to solve Eq. 5, as described below.

2.1 Input parameters

2.1.1 Gravity terms

In vertical hydrostatic equilibrium, the gravity will be balanced by the pressure. In that sense, the baryonic surface densities are one of the primary inputs which provide a significant amount of gravity into Eq. 5. Leroy et al. (2009b) observed NGC 6946 using the 30-m IRAM telescope as part of the HERACLES survey with a spatial and spectral resolution of $13.4''$ and 2.6 km s^{-1} respectively. $13.4''$ at the distance of NGC 6946 (5.9 Mpc, Karachentsev et al. (2004)) translates into a linear scale of $\sim 400 \text{ pc}$. Schruba et al. (2011) constructed the molecular surface density profile of NGC 6946 by adopting a spectral stacking technique. All the line-of-sight CO spectra within rings of width $15''$ (as obtained by the tilted ring fitting of the HI data, see de Blok et al. (2008) for more details) are stacked after shifting their centers to a common velocity. These resulting stacked spectra for different radial bins have much higher S/N than any individual line-of-sight spectrum. The molecular surface density profile is then estimated by fitting these stacked spectra. The surface density profile of the atomic gas is obtained by averaging the HI intensity distribution (as obtained by the THINGS survey) within the same tilted rings (see Schruba et al. 2011, for more details). A correction factor of 1.4 is applied to the surface density profile of the atomic gas to account for the presence of the cosmological Helium in the ISM. We adopt the stellar surface density profile of NGC 6946 as estimated by Leroy et al. (2008) using $3.6 \mu\text{m}$ data from the Spitzer Infrared Nearby Galaxy Survey (SINGS, Kennicutt et al. 2003). In Fig. 1, we show the HI (left panel) and the molecular (middle panel) maps of NGC 6946 from the THINGS and the HERACLES survey, respectively. The angular extent in both the panels is the same. Hence, it can be seen from the figure, the HI disc in NGC 6946 extends to much larger radii as compared to the molecular disc. The respective surface density profiles are shown in the rightmost panel.

Another significant source of gravity is the dark matter halo. The dark matter halo might provide a considerable amount of gravity in the vertical direction within the baryonic disc. Specifically, it could be relevant at outer radii, where the gas discs flare significantly. For NGC 6946, we use the mass-model as derived by de Blok et al. (2008). de Blok et al. (2008) fit the high-resolution rotation curve as obtained from the THINGS data with both an NFW and a pseudo-isothermal (ISO) halo. However, for NGC 6946, an ISO halo found to represent the observed rotation curve better than an NFW one. They found a characteristic core density, $\rho_0 = 45.7 \times 10^{-3} \text{ M}_{\odot} \text{ pc}^{-3}$ and a core radius, $R_c = 3.62 \text{ kpc}$ (see their Table 3 and 4 for more details). We use these two parameters to describe the dark matter halo density distribution in NGC 6946, which can be given as

$$\rho_h(R) = \frac{\rho_0}{1 + \left(\frac{R}{R_c} \right)^2} \quad (6)$$

where, $\rho_h(R)$ represents the dark matter halo density as a function of the radius.

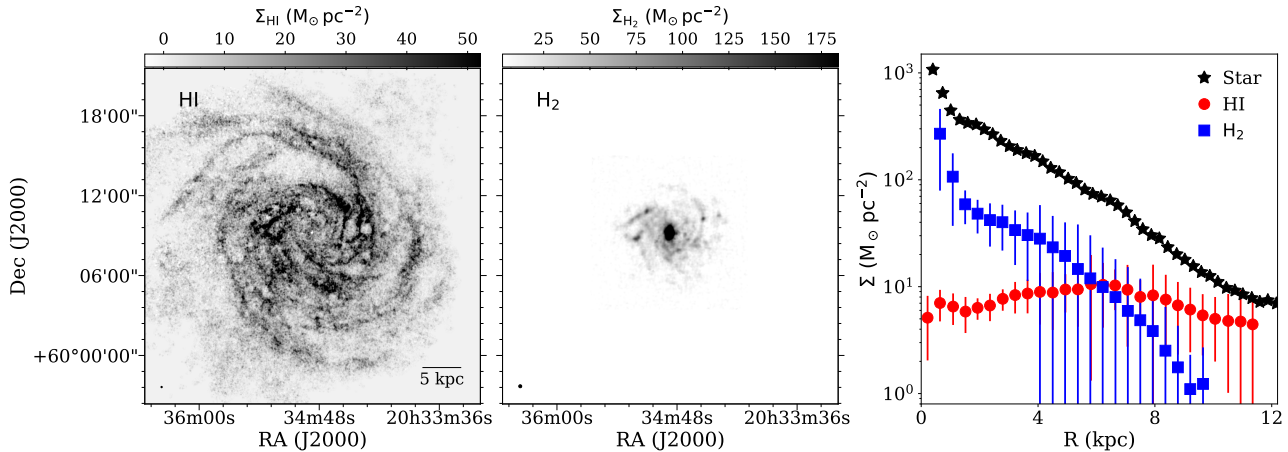


Figure 1. Left panel: The observed HI column density map of NGC 6946 (THINGS survey, Walter et al. 2008). Middle panel: The observed column density map of the molecular gas (HERACLES survey, Leroy et al. 2009b). Right panel: The surface density profiles for NGC 6946 (Leroy et al. 2008; Schruba et al. 2011). The black filled stars represent the stellar surface density profile, the solid red circles with error bars represent the HI surface density profile, whereas, the solid blue squares with error bars represent the molecular surface density profile. The observing beams are shown in the bottom left corners of the left and the middle panels. The color bars on the top of the left and the middle panels represent the column density in the units of $M_{\odot} \text{pc}^{-2}$. The left and the middle panel represents the same angular extent in the sky. As can be seen from these two panels, the HI disc extends to much larger radii as compared to the molecular disc.

2.1.2 Rotation curve

Next, the observed rotation curve acts as another essential input parameter, which is necessary to calculate the radial term, i.e., the last term on the RHS of Eq. 5. de Blok et al. (2008) used the high-resolution HI data from the THINGS survey to perform a tilted ring model fitting to the two-dimensional velocity field as obtained by a Gaussian-Hermite method. In Fig. 2, we show the rotation curve for NGC 6946. As can be seen from the figure, the rotation velocity increases as a function of the radius at the central region and flattens at $R \gtrsim 7$ kpc. It can also be seen from the figure that due to very high spatial resolution, the rotation curve exhibits significant fluctuations. However, in Eq. 5, one needs to calculate the first derivative of the squared rotation velocity to calculate the radial term. A sudden variation/jump in the rotation curve might lead to an unphysical value of this derivative and diverge the solutions of the hydrostatic equation. To avoid the same, we fit the rotation curve with a commonly used Brandt profile (Brandt 1960),

$$v_{rot}(R) = \frac{V_{max}(R/R_{max})}{\left(1/3 + 2/3 \left(\frac{R}{R_{max}}\right)^n\right)^{3/2n}} \quad (7)$$

where v_{rot} represents the observed rotation velocity at any radius, V_{max} is the maximum attained velocity, R_{max} is the radius at which V_{max} is achieved. n represents an index which signify how fast or slow the rotation curve rises as a function of the radius. For NGC 6946, a Brandt profile fit (black dashed curve in the figure) results in, $V_{max} = 199.7 \pm 0.5 \text{ km s}^{-1}$, $R_{max} = 12.0 \pm 0.6 \text{ kpc}$, and, $n = 0.69 \pm 0.05$. As can be seen from the figure, the Brandt profile fit in the central region is not steep enough. As a result, it appears to overestimates the value of R_{max} . However, we note that the radial term does not contribute to Eq. 5 considerably. Such as a value of $R_{max} = 7 \text{ kpc}$, or an exponential fit to the rotation curve (Boissier et al. 2003; Leroy et al. 2008) alters the solutions by less than one percent. Hence, we use the Brandt profile fit parameters to parametrize the rotation curve and solve the hydrostatic equation.

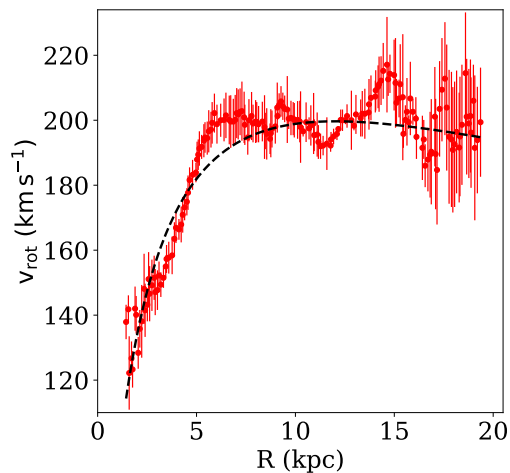


Figure 2. The rotation curve of NGC 6946. The solid red circles with error bars represent the observed rotation curve as derived by a tilted ring model fitting to the high resolution HI data from the THINGS survey (de Blok et al. 2008). The black dashed line represents a Brandt-profile fit to the data.

2.1.3 Velocity dispersion

The velocity dispersion of different baryonic components is another critical input parameters required to solve Eq. 5. The gravity on any elemental volume in the disc is contributed by all the four disc components and the dark matter halo. In that sense, a change in the surface density of any component is adjusted by all the baryonic discs. On the other hand, the velocity dispersion of an individual disc component solely decides the pressure. Thus the velocity dispersion can significantly influence the vertical structure of the baryonic discs and should be estimated precisely.

Direct measurement of the stellar velocity dispersion is difficult even with modern-day telescopes. As a result, the stellar velocity dispersion for NGC 6946 is not available. Instead, we adopt an analytical approach to estimate the stellar velocity dispersion in NGC 6946, assuming its stellar disc to be a single-

component system in vertical hydrostatic equilibrium. We use the corresponding analytical expression from Leroy et al. (2008) (see their Appendix B) to calculate the stellar velocity dispersion. It should be mentioned here that this calculation does not include the gravity due to gas discs and hence underestimates the stellar velocity dispersion. Nonetheless, the velocity dispersion of the stars does not influence the density distribution of the gas discs considerably (see, e.g., Banerjee et al. 2011a). As we are primarily interested in the distribution of the molecular gas in NGC 6946, an analytical approximation to the stellar velocity dispersion is adequate for solving the hydrostatic equation in this case.

However, unlike stellar velocity dispersion, the gas velocity dispersion in galaxies could be estimated using spectral line observations. The early low-resolution HI observations in spiral galaxies revealed an HI velocity dispersion (σ_{HI}) of 6-13 km s^{-1} (Shostak & van der Kruit 1984; van der Kruit & Shostak 1984; Kamphuis & Sancisi 1993). Tamburro et al. (2009) extensively studied the second moment of the high-resolution HI spectral cubes (MOM2) in a large number of spiral galaxies from the THINGS survey. They found an average σ_{HI} of $\sim 10 \text{ km s}^{-1}$ at the optical radius (r_{25}) of the galaxies. Later, Ianjamasimanana et al. (2012) used the same sample to stack the line-of-sight HI spectra to generate high SNR *super-profiles*. They found, $\sigma_{HI} = 12.5 \pm 3.5 \text{ km s}^{-1}$ ($\sigma_{HI} = 10.9 \pm 2.1 \text{ km s}^{-1}$ for galaxies with inclination less than 60°). However, though, all these studies found a significant variation in σ_{HI} within and across the galaxies.

To incorporate this variation of σ_{HI} within NGC 6946, we use its MOM2 map as obtained from the THINGS survey to estimate the σ_{HI} profile. In Fig. 3 top panel, we show the corresponding MOM2 map. The MOM2 profile is determined by averaging MOM2 values within radial annuli of widths \sim twice the beam size. A typical annulus at $R = 10 \text{ kpc}$ is shown in the figure (red ellipses). Thus produced MOM2 profile is shown in the bottom panel of the figure (solid red circles with error bars). The error bars indicate one-sigma scatter in MOM2 within an annulus normalized by the square root of the number of independent beams within that annulus.

As the MOM2 is the intensity weighted σ_{HI} along a line-of-sight, it always overestimates the intrinsic HI velocity dispersion (due to spectral blending). To investigate the degree of spectral blending in NGC 6946, we produce simulated MOM2 using the observed MOM2 as input σ_{HI} in Eq. 5. Using the density solutions of Eq. 5 (see §3 and §4) and the observed rotation curve, we build a three-dimensional dynamical model of the HI disc in NGC 6946. This HI disc is then inclined to the observed inclination, projected to the sky plane, and convolved with the telescope beam to produce an HI spectral cube. A simulated MOM2 profile is then computed using this spectral cube, which is shown by the empty blue triangles in the bottom panel of Fig. 3. As can be seen, the simulated and the observed MOM2 matches with each other very well, indicating a minimal spectral blending (see Patra 2020b, for more details). Hence, for NGC 6946, we use the observed MOM2 profile as the intrinsic σ_{HI} to solve Eq. 5.

In the Milky Way, observationally, it has been found that the low-mass molecular clouds show higher velocity dispersion ($\sigma_{CO} \sim 9 \text{ km s}^{-1}$) as compared to the high-mass clouds ($\sigma_{CO} \sim 6.6 \text{ km s}^{-1}$) (Stark 1984; Stark & Lee 2005). Caldú-Primo et al. (2013) stacked line-of-sight CO and HI spectra within radial bins in 12 nearby large spiral galaxies using the data from the HERACLES and the THINGS survey respectively. They estimate the spectral width profiles in these galaxies by fitting these stacked spectra by single-Gaussian functions. Thus they find a $\sigma_{HI}/\sigma_{CO} = 1.0 \pm 0.2$. Later, Mogotsi et al. (2016)

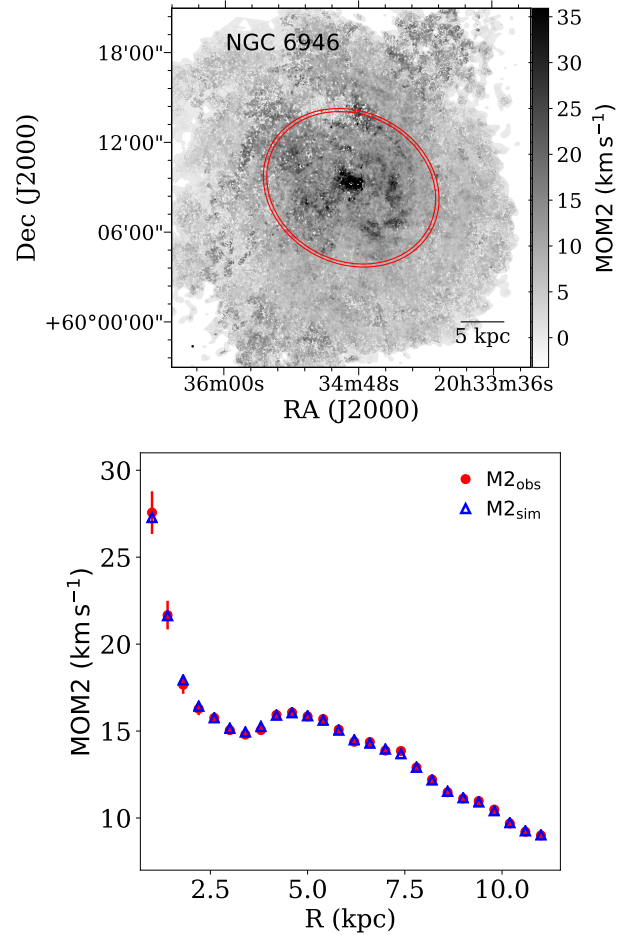


Figure 3. Top panel: Shows the MOM2 map of NGC 6946 as obtained using the THINGS survey data. The grayscale represents the observed MOM2 calculated by taking the second moment of the HI spectral cube. The red elliptical annular region represents a typical ring at a galactocentric distance of $\sim 10 \text{ kpc}$, within which the observed MOM2 values are averaged to estimate the MOM2 profile. The telescope beam is shown by the solid black circle at the left bottom corner of the panel. The bottom panel shows the MOM2 profile for NGC 6946 using the map at the top panel. The solid red circles with error bars represent the observed MOM2, whereas the empty blue triangles are the simulated MOM2 with observed MOM2 as input σ_{HI} .

investigated individual high SNR CO spectra in the same sample of galaxies and found a $\sigma_{HI}/\sigma_{CO} = 1.4 \pm 0.2$ with a $\sigma_{CO} = 7.3 \pm 1.7 \text{ km s}^{-1}$. These studies conclude that the molecular disc has two components, a thin disc that is bright and detected in the individual spectra of Mogotsi et al. (2016) and has a velocity dispersion of $\sim 7 \text{ km s}^{-1}$. The other component is diffuse and has a much lower density, which is not detected in the individual spectrum of Mogotsi et al. (2016) but discovered in the stacked spectra of Caldú-Primo et al. (2013). This component has a velocity dispersion roughly equivalent to that of the HI. Given these results, we use a $\sigma_{CO} = 7 \text{ km s}^{-1}$ for the thin disc molecular gas and a $\sigma_{CO} = \sigma_{HI}$ for the thick disc molecular gas to solve Eq. 5.

2.1.4 Thick disc molecular gas fraction

The fractional amount of molecular gas in the thin or the thick disc of NGC 6946 is not known, which we try to estimate in this work. In fact, a handful of studies to date directly estimates the thin or thick disc molecular gas fraction in galaxies. Pety et al.

(2013) used the observations from the PdBI interferometer and the 30 m single-dish IRAM telescope to compare the detected CO fluxes in the nearby spiral galaxy M51. They found a flux discrepancy (higher flux recovery in the single-dish measurement) in both the observations and attributed it to the diffuse nature of the thick disc molecular gas, which has resolved out in the interferometric observation. They concluded that at least 50% of the molecular gas in M51 is in the thick disc. However, this kind of study requires both the interferometric and single-dish observations. Not only that, but the interferometric observation also must have a high spatial resolution (was ~ 40 pc for M51). Such observational requirements are expensive and very often not possible to achieve except for very nearby galaxies. Here we use a different approach to estimate the thick/thin disc molecular gas fraction in NGC 6946, which could be applied more universally to other galaxies using existing observations. For this study, we do not consider the thick disc molecular gas fraction (f_{tk}) in NGC 6946 as constant. Instead, we solve the hydrostatic equilibrium equation allowing the f_{tk} to vary from 0.05 to 0.95 in steps of 0.05. For all f_{tk} values, we solve Eq. 5 and generate the density solutions. Using these solutions, we produce observables for all the cases and compare them individually with the observed data to estimate the f_{tk} profile, which explains the observation best.

3 SOLVING THE HYDROSTATIC EQUATION

Eq. 5 represents four coupled second-order partial differential equations in ρ_s , ρ_{HI} , $\rho_{H2,tn}$, and $\rho_{H2,tk}$. This equation cannot be solved analytically even for a two-component system. Hence, we solve Eq. 5 numerically using 8th order Runge-Kutta method as implemented in the python package `scipy`. We adopt a similar strategy as used in our previous works (Banerjee et al. 2011b; Patra 2018b, 2019). We refer the readers to these papers for a detailed description of the numerical method we use to solve the hydrostatic equilibrium equation. Here we describe the basic strategy in brief.

As Eq. 5 is a second-order differential equation, one needs at least two initial conditions to solve the equation. We choose the initial conditions as follows.

$$(\rho_i)_{z=0} = \rho_{i,0} \quad \text{and} \quad \left(\frac{d\rho_i}{dz}\right)_{z=0} = 0 \quad (8)$$

Due to the symmetry of the problem, there should be a density maxima (and hence maximum gravitational potential) at the midplane. This results in the second condition in the above equation. However, the first condition requires prior knowledge of the midplane density ($(\rho_i)_{z=0}$) for all the disc components, which is not available. We solve this problem by using the knowledge of the observed surface density. While solving Eq. 5 for any component, we start with a trial midplane density, $\rho_{t,0}$ and generate the solutions, $\rho_t(z)$. This solution is then integrated to obtain the trial surface density, $\Sigma_t = 2 \times \int \rho_t(z) dz$. This Σ_t is then compared with the observed surface density to update the trial $\rho_{t,0}$ in the next iteration. Thus, we iteratively approach to a right $\rho_{t,0}$, which produces the observed surface density within 0.1% accuracy.

Eq. 5 represents four coupled differential equations, which should be solved simultaneously. However, as the exact mathematical form of the gravitational coupling is not known, we adopt an iterative approach to introduce the coupling while solving the equations. In the first iteration, we solve individual equations (for stars, HI, thin disc molecular gas, and thick disc molecular gas) without any coupling. This results in density solutions

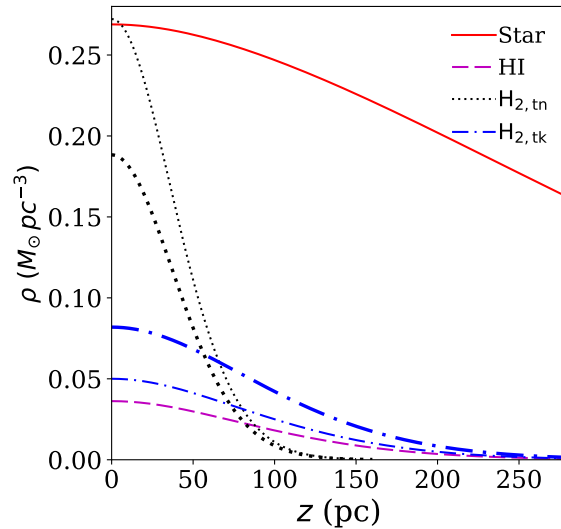


Figure 4. Sample density solutions of the hydrostatic equilibrium equation for NGC 6946 at $R=3$ kpc. The thin lines represent the solutions for a thick disc gas fraction of 0.3, whereas the thick lines represent solutions for a thick disc molecular gas fraction of 0.5. The solid red line represents the density solution for stars; the magenta dashed line depicts the solution for HI. The dotted and the dashed-dotted lines denote the density solutions for the thin and the thick disc molecular gas. As can be seen from the figure, the thick disc molecular gas extends further in the vertical direction as compared to the thin disc.

that did not consider the gravity of the other disc components. In the successive iterations, while solving for an individual component, we introduce the density solutions of the other disc components from the previous iteration into the gravity term. Thus, the density solutions grow slightly better than what was obtained in the previous iteration. We continue this iterative method until the solutions of all the components converge to better than 0.1% accuracy. We emphasize that all the codes are implemented using MPI based parallel coding for faster computation. For more details, we refer the readers to Narayan & Jog (2002); Banerjee et al. (2011a); Patra (2018b, 2019, 2020a,b,c).

4 RESULTS AND DISCUSSION

4.1 Density solutions

Adopting the technique mentioned above, we solve Eq. 5 for NGC 6946 in every 100 pc at radius, $0.7 \geq R \geq 9.5$ kpc. As the spatial resolution of the molecular data is ~ 400 pc, a radial sampling of 100 pc should be adequate to capture the density variation of the molecular disc in full details. Due to the enhanced star formation and other energetic activities at the central regions of galaxies, a hydrostatic equilibrium condition might not be prevalent in these regions. As a signature, the spectral width in these regions can attain very high values due to higher turbulent and non-circular motions. For NGC 6946, the HI spectral width at the central region reaches up to ~ 50 km s^{-1} . To avoid this problem, in NGC 6946, we exclude a central region of ~ 700 pc and do not solve Eq. 5 at $R \leq 700$ pc.

In Fig. 4, we plot sample solutions of Eq. 5 for NGC 6946 at a radius of 3 kpc. As can be seen from the figure, the stellar disc (solid red line) reaches much larger heights as compared to the HI (magenta dashed line) or the molecular discs (thin dotted and dashed-dotted lines). It can also be seen from the figure that the molecular gas in the thick disc (thin dashed-dotted lines) ex-

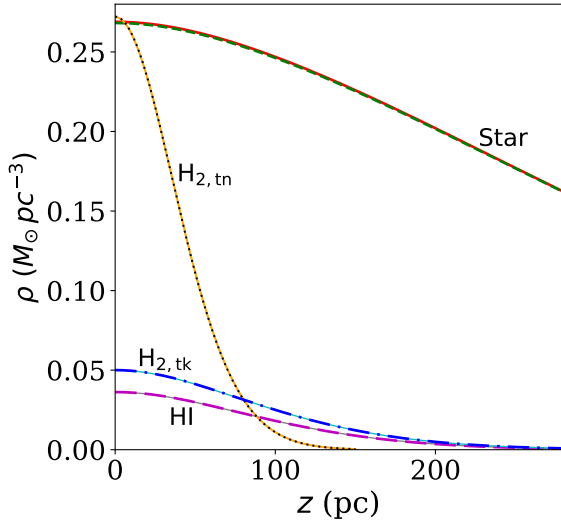


Figure 5. Density solutions at $R=3$ kpc for a lagging disc with a rotational velocity gradient of $30 \text{ km s}^{-1} \text{ kpc}^{-1}$. For comparison, the solutions for a disc without any lag is also plotted. The solid red, dashed magenta, dotted black, and dashed-dotted blue lines represent the density solutions for stars, HI, thin, and thick disc molecular gas for a galactic disc with no lag. The dashed green, solid grey, solid orange, and solid cyan lines represent the same for a lagging disc. As can be seen, the solutions of Eq. 5 do not change considerably due to the lag in the rotation curve in the vertical direction.

tends to much larger heights than the molecular gas in the thin disc (thick dotted lines). These density solutions (thin lines) are estimated for a $f_{\text{tk}} = 0.3$. For comparison, we also plot the density solutions of the molecular discs for a $f_{\text{tk}} = 0.5$ (thick lines). As can be seen, for a different f_{tk} , the density distribution of the molecular discs in the vertical direction changes significantly. Consequently, it can produce very different observational signatures in the surface density maps or in the CO spectral cubes. We note that for an individual component in hydrostatic equilibrium without any coupling, the density solutions follow a sech^2 law (see, e.g., Bahcall 1984b,a). However, due to coupling between the disc components, the exact solutions deviate from a sech^2 law and behave more like a Gaussian function.

4.2 Effects of lags

While solving Eq. 5, the rotation curve was assumed to be unchanged in the vertical direction. This forces the radial term (the last term on the RHS of Eq. 5) to be constant as a function of z . However, several observational studies revealed the existence of a significant amount of gas at large altitudes from the midplane. This gas is often referred to as extra-planar gas in literature (Swaters, Sancisi & van der Hulst 1997; Fraternali et al. 2002, 2005; Zschaechner, Rand & Walterbos 2015; Zschaechner & Rand 2015; Marasco et al. 2019; Haffner et al. 2009; Bizyaev et al. 2017; Levy et al. 2019). The extra-planar gas was also found to exhibit distinct kinematic signature, as they rotate slower (lag) than the disc gas close to the midplane. In fact, this vertical lag in the rotation is commonly used to identify and isolate the extra-planar gas in galaxies (see, e.g., Swaters, Sancisi & van der Hulst 1997; Schaap, Sancisi & Swaters 2000; Chaves & Irwin 2001; Fraternali et al. 2002, 2005; Zschaechner, Rand & Walterbos 2015; Zschaechner & Rand 2015; Vargas et al. 2017; Marasco et al. 2019). In such cases, a barotropic steady-state hydrostatic model (such as, by Barnabè et al. 2006; Fraternali & Binney 2006; Marinacci et al. 2010) of galactic discs would

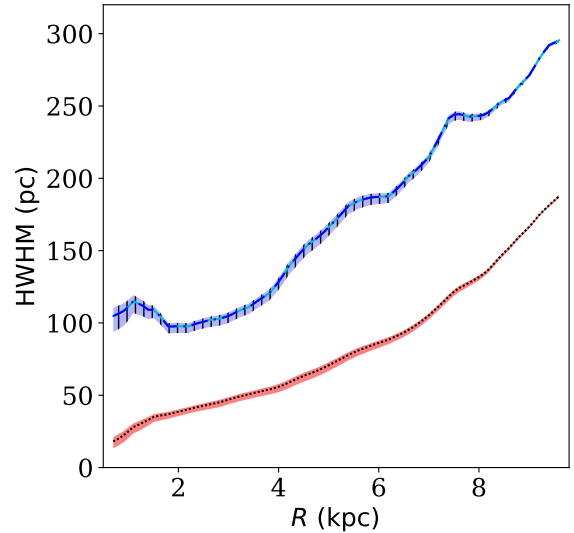


Figure 6. Show the scale height (HWHM) of different disc components as a function of radius. The red shaded region demarcates the scale height span of the thin disc molecular gas for f_{tk} between 0.3-0.9. The blue shaded region represents the scale heights of the thick disc molecular gas for the same range of f_{tk} . The hatched region shows the range of HI scale heights, which exactly matches that of the thick disc molecular gas since they have the same assumed velocity dispersion. The black dotted line represents the thin disc scale height for an $f_{\text{tk}} = 0.7$. The solid blue line and the long-dashed cyan line indicate the scale heights for the thick molecular and the HI discs, respectively (for $f_{\text{tk}} = 0.7$).

fail to capture the observed vertical lag in rotation. Instead, other mechanisms, such as anisotropic velocity dispersions (Marinacci et al. 2010) or a rotating corona (Marinacci et al. 2011), would be required to account for the observed lags. In such realistic circumstances, the assumption of a constant radial term as a function of z will not be valid fully. In fact, in NGC 6946, Boomsma et al. (2008) detected a considerable amount of extra-planar neutral gas, which exhibits the signature of a strong lag in the vertical direction. Hence, to investigate the effect of this lag on the vertical density distribution, we solve Eq. 5, introducing appropriate variation in the radial term as a function of z . For NGC 6946, the magnitude of the lag is not well quantified. Nevertheless, several previous studies have estimated the vertical lag in a number of galaxies. For example, in a recent study, Marasco et al. (2019) used sensitive HI data from the Hydrogen Accretion in LOCAL GALAXIES (HALOGAS) survey to characterize the extra-planar HI in 15 nearby galaxies. They found a typical vertical gradient in rotational velocity of $\sim -(10.0 \pm 3.7) \text{ km s}^{-1} \text{ kpc}^{-1}$. However, several studies indicate that this lag could be as large as $\sim -30 \text{ km s}^{-1} \text{ kpc}^{-1}$ for some galaxies (see, e.g., Zschaechner, Rand & Walterbos 2015; Zschaechner & Rand 2015). Adopting a conservative approach, we use a lag of $-30 \text{ km s}^{-1} \text{ kpc}^{-1}$ in Eq. 5 and examine its effect on the vertical density distribution. In Fig. 5 we show the resulting density solutions. As can be seen, the vertical gradient in the rotation velocity (or lag) does not have any meaningful effect ($\lesssim 0.3\%$) on the density solutions of Eq. 5. This is because the radial term only marginally contributes to Eq. 5. We chose to use solutions for a non-lagging disc in NGC 6946 for further analysis.

4.3 Scale height measurements

We further use the density solutions to estimate the HI and molecular scale heights in NGC 6946. The scale height is de-

defined as the Half Width at Half Maxima (HWHM) of the vertical density distribution. In Fig. 6, we show the scale heights for the thin (red shaded region) and thick (blue shaded region) molecular discs as well as for HI (hatched region). As can be seen, the thin disc molecular scale height varies between ~ 20 pc to ~ 180 pc, whereas the same can vary between $\sim 100 - 300$ pc for the thick disc and HI. Due to the same assumed velocity dispersion, the thick disc molecular gas and the HI produces the same scale heights as a function of radius. The scale heights of all the disc components flares as a function of radius and show a strong trend.

We find that our estimated molecular scale heights in NGC 6946 are \sim factor of two higher than what is observed in the Galaxy (in the same radial range). The molecular scale height in the Galaxy is found to vary between $20 - 80$ pc in the inner disc, $R \lesssim 10$ kpc (Sanders, Solomon & Scoville 1984), whereas the same flares up to $\sim 100 - 200$ pc at the outer radii (Grabelsky et al. 1987). In these regions, the molecular scale height closely matches the HI scale heights (see, e.g., Sordroski et al. 1987; Wouterloot et al. 1990; Kalberla & Dedes 2008; Kalberla & Kerp 2009). Nevertheless, our estimated scale heights for NGC 6946 is found to be consistent with several external galaxies. For example, Scoville et al. (1993) performed a CO aperture synthesis observation on the edge-on galaxy NGC 891 using the Owens Valley Millimeter Array with a spatial resolution of $\sim 2.3''$ (106 pc). They estimated the molecular scale height in this galaxy to be ~ 80 pc at the center, which increases to ~ 140 pc at the outermost radius of their measurement, i.e., ~ 10 kpc. Their measurements are consistent with our estimates of thin molecular disc scale heights. Further, Garcia-Burillo et al. (1992) used single-dish measurements with a larger beam of $\sim 13''$ (~ 600 pc) in NGC 891 to find a larger molecular scale height of $\sim 200 - 300$ pc, which is consistent with the scale heights of our thick disc molecular gas. Due to the diffuse nature of the thick disc gas, it is expected to be resolved out in the interferometric observation of Scoville et al. (1993).

Recently, (Bacchini et al. 2019) employed the hydrostatic equilibrium condition in a number of disc galaxies to determine the volume densities of different disc components along with star formation rates. Using these volume densities, they calculated the molecular and HI discs' scale height profiles in NGC 6946 (their Fig. 4). Their estimates of the scale heights in NGC 6946 is somewhat lower than what we find here. We note that to determine the volume densities, they did not solve the hydrostatic equilibrium equation in a self-consistent manner and ignored the gravity due to gaseous discs. Further, they considered the molecular disc to a single component system and assumed its velocity dispersion to be half that of the HI. The HI velocity dispersions were determined by a 3D tilted ring fitting of the HI spectral cube and parametrized by an exponential function. For NGC 6946, thus computed molecular velocity dispersion values could be as low as 3 km s^{-1} at radii $\gtrsim 5$ kpc. This is \sim two times lower than what we have assumed for the thin disc (7 km s^{-1}). This implies that our scale height profiles at these radii are expected to be ~ 2 times larger than their values, which we observe here.

Moreover, the HI scale height (same as the thick disc scale height) we find here for NGC 6946 is also consistent with other measurements in external galaxies. For example, early deep HI observations of NGC 891 reveals the existence of HI to significantly large heights from the midplane (Swaters, Sancisi & van der Hulst 1997, see also, Oosterloo, Fraternali & Sancisi (2007)). Zschaechner & Rand (2015) used the Very Large Array (VLA) to observe the HI in the edge-on galaxy NGC 4013. By using a tilted ring model fitting to the observed HI spectral cube, they estimated an upper limit to the HI scale height to be ~ 280

pc at the central region, which increases to ~ 1 kpc at radii $\gtrsim 7$ kpc. Further, detailed kinematic modeling of HI in several edge-on galaxies using HALOGAS survey data allowed estimation of HI extent in the vertical direction (Kamphuis et al. 2013; Zschaechner et al. 2012; Zschaechner, Rand & Walterbos 2015). These studies found the HI scale height in these galaxies to be a few hundred parsecs, which compares very well with what we estimated for NGC 6946.

The scale heights in NGC 6946 can vary depending on the assumed thick disc molecular gas fraction, f_{tk} . The shaded and the hatched regions in Fig. 6 depict the variation of the scale heights for the molecular and HI discs for f_{tk} values between 0.3-0.9. As can be seen from the figure, for different f_{tk} , the molecular scale height (thin or thick disc) changes by a few tens of parsecs. This, in turn, might not produce a significant difference in the total intensity (surface density) map, even for an edge-on orientation. Hence, an extremely high spatial resolution (tens of parsecs) would be required to distinguish molecular discs due to different f_{tk} , which often is not available.

4.4 Spectral cubes and width profiles

Next, we use the density solutions, observed rotation curve, and the velocity dispersion profiles to construct a three-dimensional dynamical model of the molecular disc in NGC 6946. To do that, we construct a 3D grid with 1000 cells in each dimension. We chose a cell size of 25 pc, which is sufficient to enclose the molecular disc entirely (~ 19 kpc in diameter) and adequate to sample the molecular disc with sufficient density. We interpolate the molecular gas density (both thin and thick disc), rotation velocity, and velocity dispersions in this grid to create a complete 3D dynamical model. This grid is then inclined to the observed inclination (33° , de Blok et al. (2008)), projected into the sky plane, convolved with the telescope beam ($13.4'' \times 13.4''$, Leroy et al. (2009b)), and sampled to the observed velocity resolution of 2.6 km s^{-1} (Leroy et al. 2009b) to produce an observation equivalent CO spectral cube. We repeat this exercise for molecular discs with different assumed f_{tk} and consecutively produce several CO spectral cubes. These spectral cubes are then compared with the observed one to investigate the properties of the thin and the thick molecular discs in NGC 6946.

Using the same definition as used by Caldú-Primo et al. (2013), we define the spectral width of a spectrum as the width (sigma) of a single-Gaussian function fitted to it. We use the same strategy to estimate the spectral widths in the simulated CO discs, as adopted by Caldú-Primo et al. (2013), (see also, Patra 2018a, 2020a). We first identify all the synthetic spectra within a radial bin of width equal to the observing beam. These spectra are then fitted with Gaussian-Hermite Polynomials of order three to locate their centroids. All the centroids of the spectra are then shifted to a common velocity. This, in turn, aligns all the spectra, after which we stack them to produce a stacked spectrum. Thus we produce several stacked spectra for all the radial bins. These stacked spectra are then fitted with single-Gaussian functions to estimate the spectral widths. Using the observed CO spectral cube (from the HERACLES survey), we estimate the stacked SNR in the same radial bins of our synthetic cube. Subsequently, we add an equivalent amount of noise to the simulated stacked spectra. These stacked spectra now can be considered to be observation equivalent. We bootstrap the stacked spectrum at every radial bin by producing its 1000 realizations with the same noise properties (but different noise values). All these 1000 spectra are then fitted with single-Gaussian functions. The standard deviation of their widths is then added to the fitting error in quadrature to estimate the error on the spectral width at a radial bin. Thus we

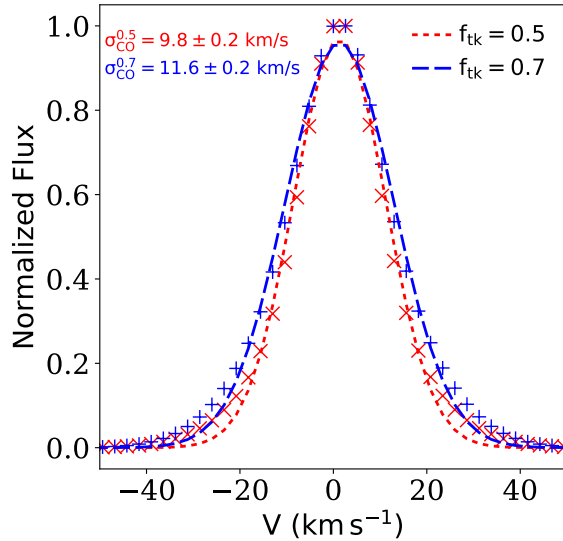


Figure 7. Simulated normalized stacked CO spectra for NGC 6946 at a radius of ~ 6 kpc. The red crosses represent the stacked spectrum for a $f_{\text{tk}} = 0.5$, whereas the blue pluses denote the same for a $f_{\text{tk}} = 0.7$. Single-Gaussian fits to the spectra are also shown by the red and the blue dashed lines, respectively. The corresponding σ_{CO} values for thick disc molecular gas fraction of 0.5 and 0.7 are found to be 9.8 km s^{-1} and 11.6 km s^{-1} , respectively.

produce a spectral width profile from a simulated spectral cube. Several such spectral width profiles are generated for molecular discs with different assumed f_{tk} . In Fig. 7, we show two representative stacked spectra for different f_{tk} of 0.5 (red crosses) and 0.7 (blue pluses) at a radius of ~ 6 kpc. For better comparison, we normalize both the spectra to unity. Single-Gaussian fits to the spectra are shown by the broken lines in the figure. As can be seen, different f_{tk} values result in stacked spectra with different spectral widths. We find a $\sigma_{\text{CO}} = 9.85 \pm 0.18 \text{ km s}^{-1}$ for $f_{\text{tk}} = 0.5$ and a $\sigma_{\text{CO}} = 11.65 \pm 0.19 \text{ km s}^{-1}$ for $f_{\text{tk}} = 0.7$ which are readily distinguishable. As can also be seen from the figure, single Gaussian fits to the stacked spectra fail to capture the broad wings produced by the thick disc molecular gas. In that sense, a single Gaussian fit would be less sensitive to the presence of thick disc molecular gas in a spectrum. To examine the same, we fitted double Gaussian profiles to the stacked spectra and used the broad component’s width as an indicator of the thick disc molecular gas fraction. However, we find that a double Gaussian fitting deblends the thin and thick disc’s spectral widths. As a result, the width of the broad component (or the narrow component) renders the CO velocity dispersion insensitive to f_{tk} and so isn’t used here. In Fig. 8 left panel, we plot the simulated σ_{CO} profiles (empty blue circles connected by blue dashed lines) for $f_{\text{tk}} = 0.5$ to 0.95 in steps of 0.05 (though we run our simulations for $f_{\text{tk}} = 0.05 - 0.95$). For comparison, we also show the observed σ_{CO} profile (solid red stars connected by an unbroken red line) as estimated by Caldú-Primo et al. (2013). As can be seen from the panel, our choice of f_{tk} values produces simulated σ_{CO} such as it encloses the observed σ_{CO} completely.

4.5 CO velocity dispersion and thick disc fractions

Next, using the simulated σ_{CO} profiles, we perform a χ^2 optimization at every radial point (defined by the radius of the observed σ_{CO}) and search for the thick disc molecular gas fraction, f_{tk} which produces a σ_{CO} closest to the observed value at that radius. Thus we obtain the f_{tk} values as a function of radius,

which produces a σ_{CO} profile best matched to the observed one. It should be mentioned here that, as the spectral widths are evaluated in bins a beam apart, and the spectral blending in NGC 6946 is minimal, there is no considerable correlation between the spectral widths in consecutive radial bins. Hence, the best fit f_{tk} value can be retrieved in every radial bins separately. In the middle panel of Fig. 8, we show thus obtained the best simulated σ_{CO} profile (empty blue circles connected with a blue dashed line) along with the observed one (solid red stars connected by an unbroken red line). As can be seen from the panel, the simulated and the observed σ_{CO} profiles match closely, indicating satisfactory modeling of the molecular discs in NGC 6946. The corresponding best fit f_{tk} profile is plotted in the right panel of Fig. 8. The optimized f_{tk} was found to vary between 0.6-0.95 with a mean value of 0.70 ± 0.09 . As can be seen from the panel, the f_{tk} values in NGC 6946 across its molecular disc appears to be consistent with the mean value with a minimal variation. To test its dependence on the radius quantitatively, we evaluate the Spearman rank correlation coefficient. We find the correlation coefficient to be 0.6. This indicates a moderate increment of f_{tk} as a function of radius.

This result is consistent with the finding of Pety et al. (2013), where they concluded at least 50% of the molecular gas in M51 is in the thick disc. Not only the thick disc molecular gas fraction, but the molecular scale height we find here (20-300 pc, Fig. 6) for NGC 6946 is also consistent with what was found by Pety et al. (2013) for M51. In an earlier study, however, Garcia-Burillo et al. (1992) observed the edge-on galaxy NGC 891 in CO and found the extent of its molecular disc to be up to 1-1.4 kpc from the midplane. A Gaussian fitting to the observed intensity profile in the vertical direction results in a vertical scale height of ~ 600 pc, which is ~ 2 times larger than what we find here. Garcia-Burillo et al. (1992) estimated the amount of molecular gas in the thick disc to be $\sim 20\%$ of the total gas content in NGC 891. However, they also point out that $\sim 40\%$ - 60% gas in NGC 891 should be in the form of low density, high velocity dispersion to explain the typical ratio of the $^{12}\text{CO} (1 \rightarrow 0)$ to $^{13}\text{CO} (1 \rightarrow 0)$ brightness. Later, Sofue & Nakai (1993) imaged NGC 891 in more detail and found CO emissions at heights of ~ 3.5 kpc from the center. They concluded that the amount of thick disc molecular gas in NGC 891 could be as high as 50%. Roman-Duval et al. (2016) used ^{12}CO and ^{13}CO observations of the Galaxy to find $\sim 10 - 20\%$ of the total molecular gas in the diffused state inside a radius of $\sim 3 - 4$ kpc, whereas this fraction increases to $\sim 50\%$ at $R \sim 15$ kpc. Further, in a recent study, Maeda et al. (2020) used ^{12}CO observations of the bar region in the galaxy NGC 1300 to find $\sim 75 - 90\%$ of the molecular gas in the diffuse thick disc. This fraction reduces to $\sim 30 - 65\%$ in the arm and bar-end region. Our result of $\sim 70 \pm 09\%$ thick disc molecular gas in NGC 6946 thus largely consistent with these previous studies.

4.6 Origin of extra-planar molecular gas

The estimation of the thick disc molecular gas fraction has many implications. For example, one can estimate the amount of extra-planar molecular gas in NGC 6946. The extra-planar molecular gas (E_{H_2}) is defined as the gas, which lies above twice the scale height of the thin disc (see, e.g., Marasco & Fraternali 2011). We use the optimized density solutions (taking care of the appropriate optimized f_{tk} at every radius) to estimate the thin disc molecular scale height at every radius and calculate the fractional amount of the molecular gas above twice this scale height. In Fig. 9 top panel, we show the distribution of the molecular gas (thin+thick) in the $R-z$ plane. The thin (solid red line) and thick

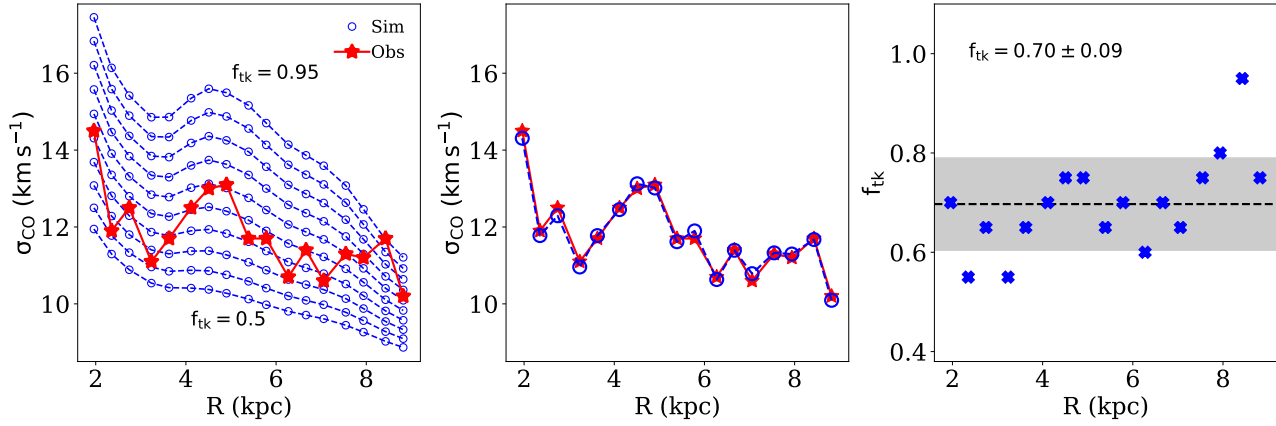


Figure 8. The left panel shows the comparison of the simulated σ_{CO} profiles with the observed one for NGC 6946. The solid red stars represent the observed σ_{CO} as obtained by stacking the CO spectra by Caldú-Primo et al. (2013). The empty blue circles represent the simulated σ_{CO} profiles for different assumed thick disc molecular gas fraction. The simulated σ_{CO} profile at the top is for a $f_{tk} = 0.95$ and the bottom one is for $f_{tk} = 0.5$. In between, the profiles are for a f_{tk} values separated by 0.05. The middle panel shows the best fit simulated σ_{CO} profile. The solid red stars represent the observed σ_{CO} profile, whereas the empty blue circles show the best fit simulated profile. Right panel: Shows the thick disc molecular gas fraction at every radial bin, which produces a simulated σ_{CO} profile that matches the observation best. The black dashed line represents the mean $f_{tk} = 0.70$, whereas the gray shaded region represents the $1-\sigma$ error on this mean value (0.09). As can be seen, our estimated f_{tk} values show a moderate incremental trend as a function of radius (with a Spearman rank correlation coefficient of 0.6, see the text for more details).

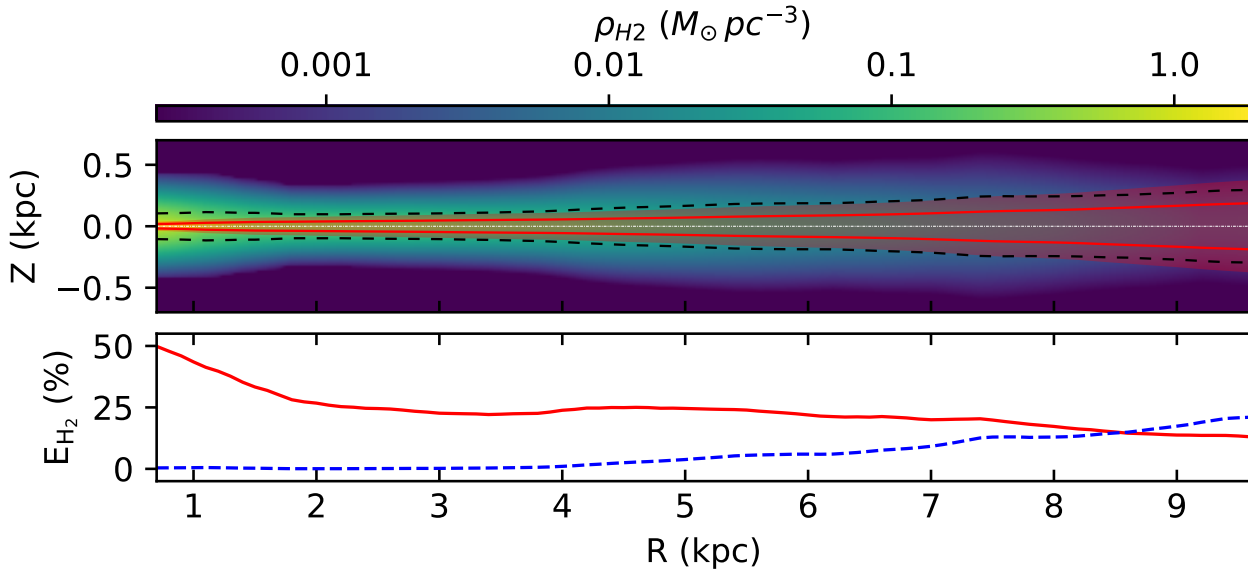


Figure 9. Top panel: The color scale shows the distribution of the molecular gas in the vertical direction as a function of radius. The white dotted line represents the midplane. The solid red lines and the dashed black lines represent the thin and thick disc scale heights, respectively. The red shaded region encloses twice the scale height of the thin disc. Any molecular gas outside this region is considered extra-planar. Bottom panel: The fractional amount of extra-planar molecular gas as a function of radius. The solid red line represents the extra-planar molecular gas fraction adopting twice the thin disc scale height, as shown in the top panel, whereas the blue dashed line indicates the fraction for a constant scale height of 300 pc.

(black dashed line) disc scale heights are also shown. The red shaded region demarcates twice the thin disc scale height. Any molecular gas outside this region is considered extra-planar. It can be seen from the figure that the amount of E_{H_2} at any radius strongly depends on the molecular scale height (of the thin disc) at that radius. The bottom panel of the figure shows the E_{H_2} fraction as a function of radius. At inner radii, much lower scale heights result in a significantly high E_{H_2} fraction. Whereas, at outer radii, the E_{H_2} fraction steadily decreases with increasing scale height. For NGC 6946, E_{H_2} fraction vary from $\sim 50\%$ at the inner radii to $\sim 15\%$ at the outer radii with a mean of $23.3 \pm 7.5\%$. For comparison, we also estimate the E_{H_2} frac-

tion (blue dashed line in the bottom panel of Fig. 9) for a constant scale height of 300 pc (scale height of the thin disc molecular gas in NGC 891, Sofue & Nakai (1993)). As can be seen, the E_{H_2} fraction for this case increases as a function radius from less than a few percent at the inner radii to $\sim 20\%$ at the edge of the molecular disc. This indicates that the flaring of the molecular disc should be taken into account while estimating the E_{H_2} fraction. Using the thin disc scale height profile to define E_{H_2} , we find that the thick disc dominantly contributes to the extra-planar molecular gas. The thin disc only contributes $\sim 5\%$ at the inner disc, which increases to $\sim 20\%$ at the edge.

To further investigate how the total molecular mass in NGC

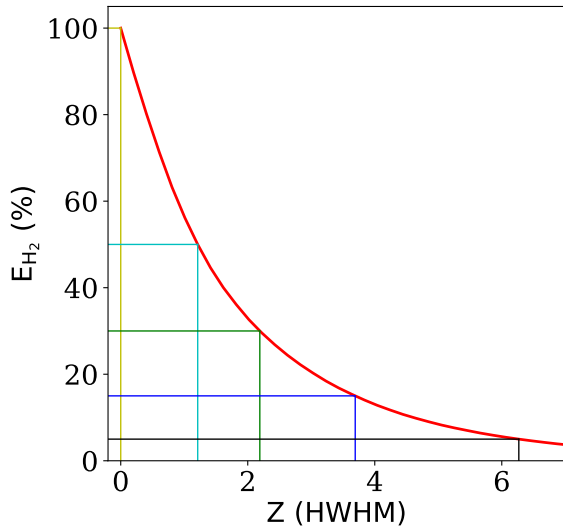


Figure 10. Fractional molecular mass in NGC 6946 above an altitude. The solid red line represents the fraction of the total molecular mass (for the entire galaxy) located above a given altitude, Z measured in the units of the thin disc scale height. The yellow, cyan, green, blue, and black lines demarcate respectively altitudes where 100%, 50%, 30%, 15%, and 5% molecular gas are located. In NGC 6946, $\sim 32\%$ molecular gas is located above twice the thin disc scale height. This gas is considered to be extra-planar.

6946 is distributed above the plane, in Fig. 10, we plot the total molecular gas fraction above an altitude (defined in the units of the thin disc scale height). This represents the cumulative fraction of the molecular gas considering contributions from all radii. In NGC 6946, we find that $\sim 32\%$ of the total molecular gas is located above twice the thin disc’s scale height. This fraction steadily decreases and falls below 10% above an altitude of ~ 4 times the thin disc scale height. This extra-planar molecular gas fraction is consistent with what is found by Pety et al. (2013). They found that $\sim 33\%$ of the total molecular gas in M51 is located above an altitude twice the thin disc (dense gas in their description) scale height (see their Fig. 20). In a recent study, Marasco et al. (2019) used deep interferometric HI data from the HALOGAS survey to investigate the extra-planar neutral gas in 15 nearby galaxies. They found that the extra-planar HI is nearly ubiquitous and contributes $\sim 5 - 25\%$ to the total neutral gas in galaxies. Albeit for neutral gas, their estimated extra-planar gas fraction compares well with our results.

The origin of this thick extra-planar molecular gas, however, is not well understood. Several stellar processes in the discs of galaxies could provide possible mechanisms, e.g., galactic fountains or chimneys, to produce extra-planar gas (Shapiro & Field 1976; Bregman 1980; Putman, Peek & Joung 2012). In fact, several high-resolution studies of nearby galaxies found direct evidence of starburst-driven expulsion of molecular gas to significant heights. For example, using high resolution (~ 70 pc) observation of ^{12}CO ($1 \rightarrow 0$), Walter, Weiss & Scoville (2002) found molecular streamers in M82. These streamers are believed to be closely related to the starburst of the galaxy and can expel a significant amount of molecular gas to a height ~ 1.2 kpc from the midplane. Likewise, several other studies have also found ample evidence of starburst-driven molecular outflows reaching about a few kpc above the midplane (Weiß et al. 1999; Sakamoto, Ho & Peck 2006; Feruglio et al. 2010; Bolatto et al. 2013). Further, AGN activity in the central regions of galaxies could also play a vital role in ejecting a significant amount of molecular gas into high altitudes (Alatalo et al. 2011; Sturm et al.

2011). Though NGC 6946 does not host any AGN (Tsai et al. 2006), it shows significantly high star formation activity in its optical disc (Degioia-Eastwood et al. 1984) with signs of many HII complexes even beyond the optical (r_{25}) radius (Ferguson et al. 1998). This enhanced star formation activity could possibly explain the estimated large amount of extra-planar molecular gas. In addition to these internal sources, accretion of gas from the CGM can also be a viable mechanism to produce a substantial amount of extra-planar molecular gas (Oort 1970; Binney 2005; Fraternali et al. 2005; Kaufmann et al. 2006). In fact, Boomsma et al. (2008) studied the extra-planar HI in NGC 6946 and concluded that while stellar feedback mechanisms could explain the extra-planar HI at the inner radii, gas accretion could play a vital role in producing the same at outer radii. However, to further understand the origin and sustenance of this extra-planar/thick disc molecular gas in galaxies, one needs to perform a similar analysis as presented here to a larger sample of galaxies, which we plan to do next.

5 CONCLUSION

In conclusion, we model the molecular disc in NGC 6946 as a two-component system with a thin disc having a low velocity dispersion of 7 km s^{-1} and a thick disc with a velocity dispersion equal to that of the HI. With this, we model the baryonic disc in NGC 6946 as a four-component system consisting of a stellar disc, HI disc, and two molecular discs (thin and thick). We assume that these discs are in vertical hydrostatic equilibrium under their mutual gravity in the external force-field of the dark matter halo. Under this assumption, we formulate the Poisson-Boltzmann equation of hydrostatic equilibrium and solve it numerically using an 8th order Runge-Kutta method to obtain a three-dimensional density distribution of the baryonic discs. In particular, we investigate the three-dimensional density distribution of the molecular gas in NGC 6946 and its implications on the observed CO spectral widths.

Inspecting the solutions of the hydrostatic equilibrium equation, we find that the density of the individual disc components deviates from a conventional sech^2 law due to the coupling between the disc components. In the presence of other disc components, the density solutions behave more like a Gaussian function. We also find that for NGC 6946, the HI and the thick disc molecular gas acquires a larger scale height as compared to the thin disc molecular gas. The molecular scale height in the thin disc was found to vary between $20 - 200$ pc, whereas the same found to vary between $100 - 300$ pc in the thick disc. Due to the same assumed velocity dispersions, the thick disc molecular gas and the HI shows the same scale height.

We further use the density solutions, the observed rotation curve, and the velocity dispersion profiles to build three-dimensional dynamical models of molecular discs in NGC 6946. These dynamical models then inclined to the observed inclination, projected into the sky plane, and convolved with the telescope beam to produce observation equivalent simulated CO spectral cubes. A number of such spectral cubes are produced for different assumed f_{tk} in the molecular disc of NGC 6946. These spectral cubes are further used to produce CO spectral width profiles by stacking CO spectra within radial bins and fitting them with single-Gaussian functions. These spectral width profiles are then compared with the observed one to constrain the thick disc molecular gas fraction in NGC 6946.

Using a χ^2 method, we estimate the thick disc molecular gas fraction in NGC 6946 at all the radial bins, which produces a simulated spectral width that best matches the observation. We find that the best optimized simulated spectral width pro-

file matches the observed one very well. We also find that the corresponding thick disc molecular gas fraction profile almost remains constant (albeit with a slight sign of increasing trend) as a function of the radius with a mean value of 0.70 ± 0.09 . This means that in NGC 6946, $\sim 70\%$ of the total molecular gas is in the thick disc. *This is the first-ever estimation of the thick disc molecular gas fraction in an external galaxy as a function of the radius with sub-kpc spatial resolution.*

We also estimate the amount of extra-planar molecular gas in NGC 6946. The extra-planar molecular gas (E_{H_2}) is defined as the gas, which lies above twice the scale height of the thin disc (see, e.g., Marasco & Fraternali 2011). The fraction of extra-planar molecular gas in NGC 6946 was found to vary from $\sim 50\%$ at the center to $\sim 15\%$ at the edge of the molecular disc with a mean value of $\sim 23.3\% \pm 7.5\%$. A high fraction of the extra-planar molecular gas at the center of NGC 6946 supports the idea that this extra-planar gas could originate through different stellar feedback processes, e.g., galactic fountain or chimney. However, understanding the origin and sustenance of the thick disc/extra-planar molecular gas in galaxies would require a similar study in a larger sample of galaxies, which we plan to do next.

6 ACKNOWLEDGEMENT

This work made use of The HI Nearby Galaxy Survey (THINGS, Walter et al. (2008)) and The HERA CO-Line Extragalactic Survey (HERACLES, Leroy et al. (2009b)) data. NNP would like to thank the THINGS and the HERACLES team for making the data publicly available.

7 DATA AVAILABILITY

We used already existing publicly available data for this work. No new data were generated or analyzed in support of this research.

REFERENCES

- Alatalo K. et al., 2011, ApJ, 735, 88
 Bacchini C., Fraternali F., Iorio G., Pezzulli G., 2019, A&A, 622, A64
 Bahcall J. N., 1984a, ApJ, 276, 169
 Bahcall J. N., 1984b, ApJ, 276, 156
 Banerjee A., Jog C. J., Brinks E., Bagetakos I., 2011a, MNRAS, 415, 687
 Banerjee A., Jog C. J., Brinks E., Bagetakos I., 2011b, MNRAS, 415, 687
 Barnabè M., Ciotti L., Fraternali F., Sancisi R., 2006, A&A, 446, 61
 Bigiel F., Leroy A., Walter F., Blitz L., Brinks E., de Blok W. J. G., Madore B., 2010, AJ, 140, 1194
 Bigiel F., Leroy A., Walter F., Brinks E., de Blok W. J. G., Madore B., Thornley M. D., 2008, AJ, 136, 2846
 Binney J., 2005, Philosophical Transactions of the Royal Society of London Series A, 363, 739
 Bizyaev D. et al., 2017, ApJ, 839, 87
 Blitz L., Shu F. H., 1980, ApJ, 238, 148
 Boettcher E., Zweibel E. G., Gallagher, J. S. I., Benjamin R. A., 2016, ApJ, 832, 118
 Boissier S., Prantzos N., Boselli A., Gavazzi G., 2003, MNRAS, 346, 1215
 Bolatto A. D. et al., 2013, Natur, 499, 450
 Boomsma R., Oosterloo T. A., Fraternali F., van der Hulst J. M., Sancisi R., 2008, A&A, 490, 555
 Brandt J. C., 1960, ApJ, 131, 293
 Bregman J. N., 1980, ApJ, 236, 577
 Caldu-Primo A., Schruha A., Walter F., Leroy A., Sandstrom K., de Blok W. J. G., Ianjamasimanana R., Mogotsi K. M., 2013, AJ, 146, 150
 Chaves T. A., Irwin J. A., 2001, ApJ, 557, 646
 Cohen R. S., Cong H., Dame T. M., Thaddeus P., 1980, ApJL, 239, L53
 de Blok W. J. G., Walter F., Brinks E., Trachternach C., Oh S.-H., Kennicutt, Jr. R. C., 2008, AJ, 136, 2648
 Degioia-Eastwood K., Grasdalen G. L., Strom S. E., Strom K. M., 1984, ApJ, 278, 564
 Dettmar R. J., 1990, A&A, 232, L15
 Ferguson A. M. N., Wyse R. F. G., Gallagher J. S., Hunter D. A., 1998, ApJL, 506, L19
 Feruglio C., Maiolino R., Piconcelli E., Menci N., Aussel H., Lamastra A., Fiore F., 2010, A&A, 518, L155
 Fraternali F., Binney J. J., 2006, MNRAS, 366, 449
 Fraternali F., Oosterloo T. A., Sancisi R., Swaters R., 2005, in Astronomical Society of the Pacific Conference Series, Vol. 331, Extra-Planar Gas, Braun R., ed., p. 239
 Fraternali F., van Moorsel G., Sancisi R., Oosterloo T., 2002, AJ, 123, 3124
 Garcia-Burillo S., Guelin M., Cernicharo J., Dahlem M., 1992, A&A, 266, 21
 Grabelsky D. A., Cohen R. S., Bronfman L., Thaddeus P., May J., 1987, ApJ, 315, 122
 Haffner L. M. et al., 2009, Reviews of Modern Physics, 81, 969
 Hartmann L., Ballesteros-Paredes J., Bergin E. A., 2001, ApJ, 562, 852
 Heyer M., Dame T. M., 2015, ARA&A, 53, 583
 Hoopes C. G., Walterbos R. A. M., Rand R. J., 1999, ApJ, 522, 669
 Howk J. C., Savage B. D., 2000, AJ, 119, 644
 Ianjamasimanana R., de Blok W. J. G., Walter F., Heald G. H., 2012, AJ, 144, 96
 Jo Y.-S., Seon K.-i., Shinn J.-H., Yang Y., Lee D., Min K.-W., 2018, ApJ, 862, 25
 Kalberla P. M. W., Dedes L., 2008, A&A, 487, 951
 Kalberla P. M. W., Kerp J., 2009, ARA&A, 47, 27
 Kamphuis J., Sancisi R., 1993, A&A, 273, L31
 Kamphuis P., Holwerda B. W., Allen R. J., Peletier R. F., van der Kruit P. C., 2007a, A&A, 471, L1
 Kamphuis P., Peletier R. F., Dettmar R. J., van der Hulst J. M., van der Kruit P. C., Allen R. J., 2007b, A&A, 468, 951
 Kamphuis P. et al., 2013, MNRAS, 434, 2069
 Karachentsev I. D., Karachentseva V. E., Huchtmeier W. K., Makarov D. I., 2004, AJ, 127, 2031
 Kaufmann T., Mayer L., Wadsley J., Stadel J., Moore B., 2006, MNRAS, 370, 1612
 Kawamura A. et al., 2009, ApJS, 184, 1
 Kennicutt, Jr. R. C., 1998, ApJ, 498, 541
 Kennicutt, Jr. R. C. et al., 2003, PASP, 115, 928
 Koda J. et al., 2011, ApJS, 193, 19
 Koda J., Scoville N., Heyer M., 2016, ApJ, 823, 76
 Krieger N. et al., 2019, ApJ, 881, 43
 Leroy A. K. et al., 2009a, ApJ, 702, 352
 Leroy A. K. et al., 2009b, AJ, 137, 4670
 Leroy A. K., Walter F., Brinks E., Bigiel F., de Blok W. J. G., Madore B., Thornley M. D., 2008, AJ, 136, 2782
 Levy R. C. et al., 2019, ApJ, 882, 84
 Maeda F., Ohta K., Fujimoto Y., Habe A., Ushio K., 2020, MNRAS, 495, 3840

- Marasco A., Fraternali F., 2011, *A&A*, 525, A134
- Marasco A. et al., 2019, *A&A*, 631, A50
- Marinacci F., Binney J., Fraternali F., Nipoti C., Ciotti L., Londrillo P., 2010, *MNRAS*, 404, 1464
- Marinacci F., Fraternali F., Nipoti C., Binney J., Ciotti L., Londrillo P., 2011, *MNRAS*, 415, 1534
- Miura R. E. et al., 2012, *ApJ*, 761, 37
- Mogotsi K. M., de Blok W. J. G., Caldú-Primo A., Walter F., Ianjamasimanana R., Leroy A. K., 2016, *AJ*, 151, 15
- Narayan C. A., Jog C. J., 2002, *A&A*, 394, 89
- Oort J. H., 1970, *A&A*, 7, 381
- Oosterloo T., Fraternali F., Sancisi R., 2007, *AJ*, 134, 1019
- Patra N. N., 2018a, *MNRAS*, 480, 4369
- Patra N. N., 2018b, *MNRAS*, 478, 4931
- Patra N. N., 2019, *MNRAS*, 484, 81
- Patra N. N., 2020a, *MNRAS*, 495, 2867
- Patra N. N., 2020b, *MNRAS*, 499, 2063
- Patra N. N., 2020c, *A&A*, 638, A66
- Patra N. N., Chengalur J. N., Karachentsev I. D., Kaisin S. S., Begum A., 2016, *MNRAS*, 456, 2467
- Pety J. et al., 2013, *ApJ*, 779, 43
- Putman M. E., Peek J. E. G., Jong M. R., 2012, *ARA&A*, 50, 491
- Rand R. J., Kulkarni S. R., 1990, *ApJL*, 349, L43
- Roman-Duval J., Heyer M., Brunt C. M., Clark P., Klessen R., Shetty R., 2016, *ApJ*, 818, 144
- Rossa J., Dettmar R.-J., Walterbos R. A. M., Norman C. A., 2004, *AJ*, 128, 674
- Roychowdhury S., Chengalur J. N., Begum A., Karachentsev I. D., 2009, *MNRAS*, 397, 1435
- Roychowdhury S., Chengalur J. N., Kaisin S. S., Begum A., Karachentsev I. D., 2011, *MNRAS*, 414, L55
- Roychowdhury S., Chengalur J. N., Kaisin S. S., Karachentsev I. D., 2014, *MNRAS*, 445, 1392
- Roychowdhury S., Chengalur J. N., Shi Y., 2017, *A&A*, 608, A24
- Sakamoto K., Ho P. T. P., Peck A. B., 2006, *ApJ*, 644, 862
- Salak D., Nakai N., Miyamoto Y., Yamauchi A., Tsuru T. G., 2013, *PASJ*, 65, 66
- Salak D., Nakai N., Sorai K., Miyamoto Y., 2020, *ApJ*, 901, 151
- Sanders D. B., Solomon P. M., Scoville N. Z., 1984, *ApJ*, 276, 182
- Schaap W. E., Sancisi R., Swaters R. A., 2000, *A&A*, 356, L49
- Schmidt M., 1959, *ApJ*, 129, 243
- Schruba A. et al., 2011, *AJ*, 142, 37
- Schruba A. et al., 2012, *AJ*, 143, 138
- Scoville N. Z., Hersh K., 1979, *ApJ*, 229, 578
- Scoville N. Z., Thakkar D., Carlstrom J. E., Sargent A. I., 1993, *ApJL*, 404, L59
- Seon K.-i., Witt A. N., Shinn J.-h., Kim I.-j., 2014, *ApJL*, 785, L18
- Shapiro P. R., Field G. B., 1976, *ApJ*, 205, 762
- Shinn J.-H., 2018, *ApJS*, 239, 21
- Shostak G. S., van der Kruit P. C., 1984, *A&A*, 132, 20
- Sodroski T. J., Dwek E., Hauser M. G., Kerr F. J., 1987, *ApJ*, 322, 101
- Sofue Y., Nakai N., 1993, *PASJ*, 45, 139
- Stark A. A., 1984, *ApJ*, 281, 624
- Stark A. A., Lee Y., 2005, *ApJL*, 619, L159
- Sturm E. et al., 2011, *ApJL*, 733, L16
- Swaters R. A., Sancisi R., van der Hulst J. M., 1997, *ApJ*, 491, 140
- Tamburro D., Rix H.-W., Leroy A. K., Mac Low M.-M., Walter F., Kennicutt R. C., Brinks E., de Blok W. J. G., 2009, *AJ*, 137, 4424
- Taylor C. L., Koblunicky H. A., Skillman E. D., 1998, *AJ*, 116, 2746
- Tsai C.-W., Turner J. L., Beck S. C., Crosthwaite L. P., Ho P. T. P., Meier D. S., 2006, *AJ*, 132, 2383
- van der Kruit P. C., Shostak G. S., 1984, *A&A*, 134, 258
- Vargas C. J. et al., 2017, *ApJ*, 839, 118
- Vogel S. N., Kulkarni S. R., Scoville N. Z., 1988, *Natur*, 334, 402
- Walter F., Brinks E., de Blok W. J. G., Bigiel F., Kennicutt, Jr. R. C., Thornley M. D., Leroy A., 2008, *AJ*, 136, 2563
- Walter F., Weiss A., Scoville N., 2002, *ApJL*, 580, L21
- Weiß A., Walter F., Neiningner N., Klein U., 1999, *A&A*, 345, L23
- Wouterloot J. G. A., Brand J., Burton W. B., Kwee K. K., 1990, *A&A*, 230, 21
- Zschaechner L. K., Rand R. J., 2015, *ApJ*, 808, 153
- Zschaechner L. K., Rand R. J., Heald G. H., Gentile G., Józsa G., 2012, *ApJ*, 760, 37
- Zschaechner L. K., Rand R. J., Walterbos R., 2015, *ApJ*, 799, 61